Available online at www.sciencedirect.com
SCIENCE DIRECT®
Thermochimica Acta 402 (2003) 57–67
thermochimica acta
www.elsevier.com/locate/tca

The role of thermal analysis in optimization of the electrochromic effect of nickel oxide thin films, prepared by the sol–gel method. Part I

R. Cerc Korošec [a,*], P. Bukovec [a], B. Pihlar [a], J. Padežnik Gomilšek [b]

[a] *Faculty of Chemistry and Chemical Technology, University of Ljubljana, Aškerčeva 5, 1000 Ljubljana, Slovenia*
[b] *Faculty of Mechanical Engineering, University of Maribor, Smetanova 17, 2000 Maribor, Slovenia*

Received 30 May 2002; received in revised form 6 June 2002; accepted 29 October 2002

Abstract

Nickel oxide thin films have been widely studied as an optical active layer in electrochromic devices. It is well known for these films that thermal treatment is the key factor which determines the electrochromic effect during potential cycling. Therefore, it is extremely important to perform thermal analysis on the thin films rather than on the corresponding xerogels. In this article, the thermal behaviour of sol–gel derived nickel oxide thin films, prepared from $NiSO_4$ precursor, is compared to that of the corresponding xerogel using dynamic and isothermal TG and dynamic DSC measurements. By regulating the duration of the heat treatment at 270 °C, one can control the thermal conversion of the amorphous thin film into nickel oxide. For the xerogel, this process occurs at 300 °C. Using the EXAFS method, it was confirmed that the amorphous xerogel is analogous to the thin film sample. Thermal decomposition of the amorphous xerogel was studied in detail by IR and MS techniques. From the weight loss curve of the thin film, the substrate to film mass ratio was determined for different substrates. The effect of heat treatment on these films was determined by measuring their electrochromic properties.

Keywords: TG/DSC; NiO thin films; Electrochromism; Sol–gel; $NiSO_4$ precursor

1. Introduction

Nanostructured nickel oxide is a material showing two promising properties: high electrochromic efficiency [1] and p-type semiconductivity [2]. The latter property is of interest in the field of photoelectrochemical cells [3].

Electrochromic nickel oxide thin films, prepared by various physical and chemical methods [4–8] among which sputtering is most commonly used [9–13], differ in stoichiometry, structure, degree of crystallinity, crystallite size, etc. As a consequence, their electrochromic properties vary over a wide range. During or after the deposition process, the films have to be thermally treated in order to improve adhesion to the substrate and to ensure their structural stability during cycling in an alkaline electrolyte. Regardless of the preparation technique, the degree of thermal treatment is the key factor which influences the magnitude of the optical modulation and stability of the film during the cycling process. Too high processing temperature significantly lowers the electrochromic effect [11–14], and the layer could even become inactive [13,15,16]. On the other hand, in thermally untreated films either the optical modulation decreases soon after the

* Corresponding author.
E-mail address: romana.cerc-korosec@uni-lj.si (R. Cerc Korošec).

0040-6031/03/$ – see front matter
PII: S0040-6031(02)00537-3

beginning of cycling [17,18] or the film becomes detached from the substrate [10,19].

Chemical methods of deposition are cheaper and technically less demanding than physical ones [14,20,21]. The sol–gel method gained increasing interest during the last few years in the preparation of thin films [20,21]. It enables control of the variety of composition and homogeneity of the final product, as well as a lower processing temperature.

The thickness of thin films usually does not exceed 1 μm [22]. When the sample is prepared as a thin film or in powdered form, the differences in the particle size and in microstructure of the two forms lead to different thermal stabilities. It is well known that the decomposition temperature decreases with decrease in sample particle size [23]. Therefore, thermal decomposition of sol–gel derived thin films occurs at lower temperatures than that of xerogels [24]. Explanation of stoichiometric or structural properties of a thin film by results obtained from TG and DSC curves of xerogels could lead to a wrong interpretation.

Thermal analysis of thin films is a demanding procedure and direct measurements of thin films are still not very common [22]. This is the reason why in articles which report thin film properties the thermal analysis is either made on the corresponding xerogels [6,15,20,25,26] or the investigated films are thermally treated at 250 or 300 °C without performing TG analysis even for xerogels [14,27]. The sensitivity of balances in TG instruments is in the order of 1 μg so that detection of the thermal decomposition of thin films is possible [28]. But the amount of sample available is small, typically below 1 mg, so that the mass change during TG experiment is in the range of buoyancy and aerodynamic effects. In DSC measurements, the evolved or absorbed heat diffuses into the substrate and consequently the measured enthalpies are very small [29]. In order to overcome these problems, large area samples were used [30–32] or measurements carefully performed—for instance subtraction of the blank curve [29], high resolution TG [33] or the thin film was placed directly on the sample thermocouple in DSC measurements [34].

The aim of our work was to study comparatively the thermal behaviour of sol–gel derived nickel oxide thin films and xerogel, respectively, prepared from nickel sulfate precursor, and to optimize the thermal treatment of the films with respect to electrochromic response. As far as we know, thermal analysis of thin films has not so far been performed for this purpose.

2. Experimental

2.1. Preparation of sol

LiOH solution of 2.0 M (Kemika, Zagreb, Croatia) was added dropwise to a 0.5 M solution of nickel sulfate (Kemika, Zagreb, Croatia) until pH 9.0 was reached. The green precipitate was washed several times with water. The slurry was then peptised with glacial acetic acid to pH 4.5. Some water was added to obtain an appropriate viscosity. The sol was then sonicated and filtered [15].

2.2. Thin film deposition

Thin films were prepared on different substrates using the dip-coating technique. The substrates used for TG measurements included microscope slide glasses ($1 \times 2\ cm^2$, thickness 1 mm), microscope cover glasses and aluminium foil (thickness 0.01 mm). A small hole was previously drilled in the slide glasses, to allow the suspension of the sample on a platinum wire. For DSC measurements, a small (diameter 6 mm) home made platinum disc was used. Before deposition a wetting agent was dispersed on all types of substrates using a dip-coating technique. For glasses, a solution of 1 wt.% of Etolat TD-60 (TEOL Factory, Ljubljana, Slovenia) in distilled water was prepared and for aluminium foil or platinum disc, a solution of 1 wt.% of Teloxide (TEOL Factory, Ljubljana, Slovenia) in ethanol. After the wetting solution had dried, the thin film was deposited with a pulling velocity of $5\ cm\ min^{-1}$.

2.3. Preparation of xerogel

The sols were cast in petri dishes and left to dry. The solid xerogel consisted of two phases.

2.4. Instrumental

Dynamic thermoanalytical measurements were performed on a Perkin-Elmer TGA 7 Thermoanalyser while a Mettler Toledo TGA/SDTA 851^e instrument

was used for isothermal ones. A temperature range from room temperature up to 900 °C was applied for xerogels and from 25 to 600 °C for thin films deposited on glass substrates or Al foil. The initial mass of the xerogel was approximately 10 mg. Microscope cover glasses with deposited films were placed between two clean sheets of paper and then broken into small pieces suitable for placing into the pan. Aluminium foil was cut with scissors to similar dimensions. Platinum crucibles (diameter 8 mm) and a heating rate of 5 K min^{-1} were used in dynamic measurements. In isothermal measurements the furnace was heated at 2 K min^{-1} to the chosen temperature, left at that temperature for 90 min and then heated up to 350 °C at 2 K min^{-1}. The baseline was subtracted in all cases.

DSC analysis was carried out on a Mettler DSC 20 Cell in dynamic air atmosphere. For thin films, deposited on microscope cover glasses or aluminium foil, 40 μl sample pans were used and an empty pan served as a reference.

EGA measurements were performed on STA 409 Netzsch apparatus. Evolved gases were detected using a Leybold Heraeus Quadrex 200 mass spectrometer. The initial mass of the sample (500 mg) was weighed in a 3.4 ml alumina crucible. During the measurement the furnace was purged with air (100 ml min^{-1}). The heating rate was 5 K min^{-1}.

Ion chromatography was performed on a Merck–Hitachi System, consisted of a gradient pump (L-6200A), an autosampler (AS-2000A), a conductivity detector (Iskra MA 4110 equipped with Dionex SRS Controller and Anion Micromembrane Suppressor ASRS-ULTRA) and a data interface (D-6000) with an appropriate software (HPLC manager, version 2). Separation of sulphate anions was obtained using Dionex AS4A-SC ion chromatographic separation column combined with Dionex AG4A-SC pre-column. Eluent flow rate was set to 2 ml min^{-1}. Sulphate anions were detected by conductivity detector. All measurements were performed at room temperature. Eluent was the carbonate/hydrogen carbonate buffer with the concentrations of 1.8 and 1.7 mM, respectively. Before the measurement, the system was calibrated with four standard solutions (concentration of SO_4^{2-} ions 1, 3, 5 and 10 μg ml^{-1}).

In situ UV-Vis spectroelectrochemical measurements were made in the range 360–1100 nm using a Perkin-Elmer UV/VIS Lambda 2 Spectrometer, connected to an EG&G PAR Model 273 computer-controlled potentiostat–galvanostat. A potential scan rate of 10 mV s^{-1} was used for CV measurements. A homemade three-electrode spectroelectrochemical transmission cell, filled with a 40 ml of 0.1 M LiOH, was used. A Pt rod served as the counter electrode, an $Ag/AgCl/KCl_{sat}$ cell as the reference electrode ($E = 0.197$ V) and a thin Ni oxide film deposited on SnO_2/F glass (square resistivity 13 $\Omega/\square$) as the working electrode. For background measurements, a cell filled with only the electrolyte was used. The current densities were calculated from the active area of the films.

Thickness measurements of thin films prepared for the electrochemical measurements, were performed using a Talysurf profilometer (Taylor Hobson).

3. Results and discussion

The two phases of the xerogel (light and dark green, Fig. 1) were separated using an optical microscope and milled in an agate mortar. Powder diffraction analysis was made for each of them. Results show that the light green phase is amorphous and the dark green phase is nickel(II) acetate tetrahydrate.

Dynamic thermogravimetric curves of the xerogel and thin film are shown in Fig. 2. From 25 to 240 °C dehydration takes place (EGA analysis, Fig. 3). For the amorphous phase and the thin film, this is a gradual process whereas for the crystalline xerogel, it occurs in one step. Within this range the weight loss is 20% for the amorphous xerogel and 34.1% for the crystalline xerogel. The latter deviates from the calculated value for nickel(II) acetate tetrahydrate (28.9%) by more than 5%. The observed discrepancy will be explained later on. After dehydration thermal decomposition of acetato groups occur. The onset decomposition temperature is lower for the thin film (280 °C) than for the amorphous xerogel (300 °C)—see inserted graph in Fig. 2. In the temperature range from 240 to 360 °C, the amorphous xerogel loses 34.5% of its weight. During thermal decomposition of acetato groups the release of gases (water, CO_2) and fragments (CH_3^+, CH_3CO^+) was monitored (Fig. 3). It is evident from the IR spectra (Fig. 4) that at the same time the formation of nickel oxide takes place. In thermally untreated xerogel (Fig. 4a) acetato

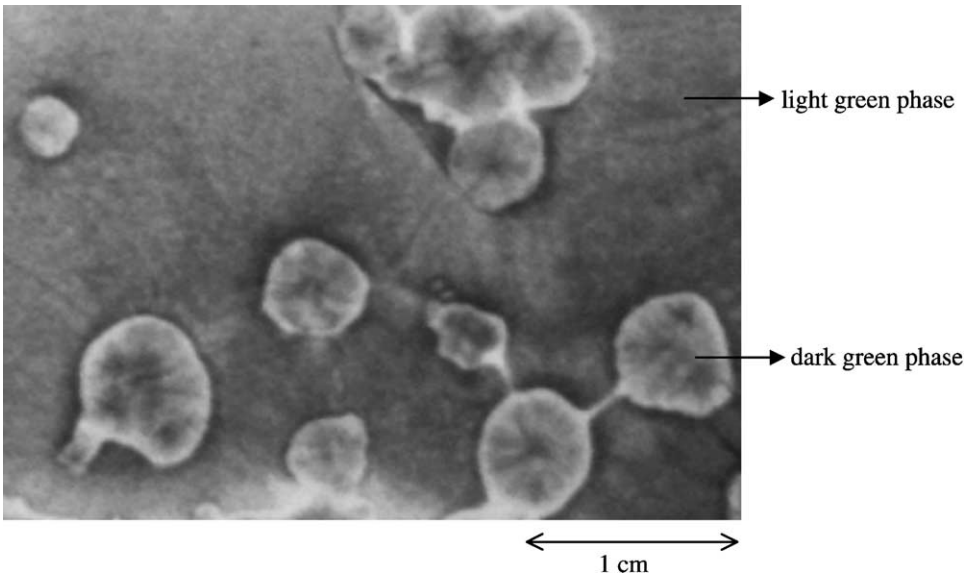

Fig. 1. Photograph of the dried sol.

(1560, 1420, 1345, 1052, 1029, 680 cm^{-1}) [35] and sulphato groups (1142, 1113–1095, 618 cm^{-1}) [36] can be identified. At 360 °C (Fig. 4b) sulfate groups (1141, 1109 cm^{-1}) and nickel oxide (443 cm^{-1}) [37] can be seen. The XRD pattern of this sample reveals the presence of Bunsenite NiO phase. The crystallite size was calculated using the Scherrer formula and is approximately 9 nm.

The third step in the thermogravimetric curve of the amorphous xerogel (weight loss of 6.2%) begins

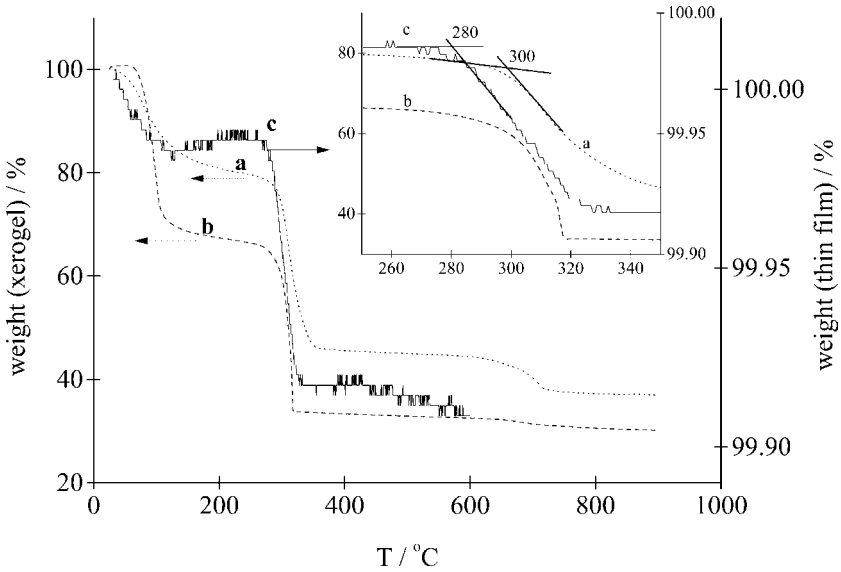

Fig. 2. Dynamic thermogravimetric curves of the amorphous (a) and crystalline xerogel (b) (left ordinate) and of a thin film deposited on a microscope cover glass (c) (right ordinate) in a dynamic air atmosphere.

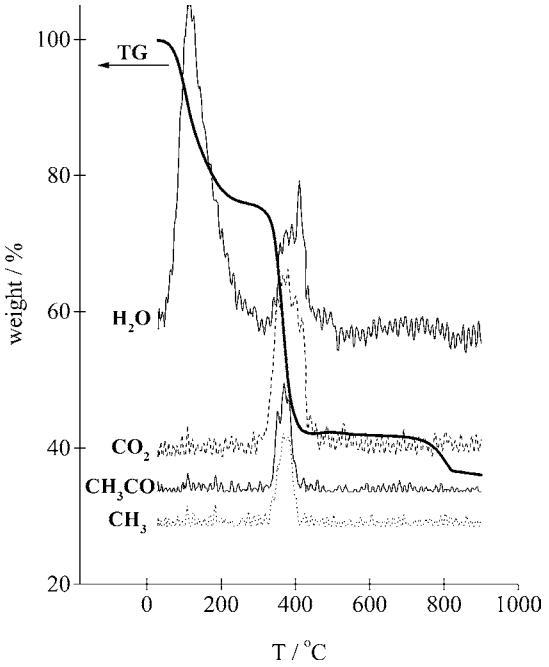

Fig. 3. TG and EGA-MS curves of the amorphous xerogel.

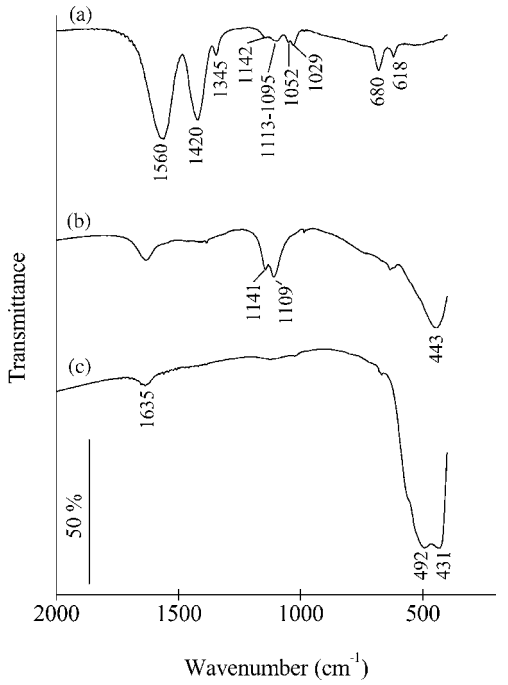

Fig. 4. IR transmittance spectra of the amorphous xerogel (a) and its residues at 360 °C (b) and 800 °C (c).

above 600 °C (Fig. 2). Some authors [6] attribute this weight loss to oxygen release leading to the formation of a perfectly stoichiometric material, according to the reaction:

$$NiO_{1+2x} \rightarrow NiO + x\,O_2.$$

But from the IR spectrum of the xerogel heat treated at 800 °C (Fig. 4c), it is obvious that sulphato groups are no longer present in the sample. Therefore, we attribute this weight loss to thermal decomposition of sulphato groups, although within this temperature range we did not detect any gases in EGA analysis due to sulphur release (*m/z*: 80, SO_3^+; 64, SO_2^+; 48, SO^+ or 24, SO^{2+}). They may condense in the heated leak which connects the thermoanalyzer to the mass spectrometer.

The presence of sulphate ions was proved using ion chromatography. Amorphous xerogel (7.19 mg) was dissolved in triple distilled water. The final volume of the solution was 100 ml. The calculated value of SO_4^{2-} ions in the prepared sample was 5.35 μg ml^{-1}. The result obtained by ion chromatography was 5.50 μg ml^{-1}. The observed discrepancy is within the experimental error.

The weight loss of 1.8% of the crystalline xerogel sample in the temperature range from 600 to 800 °C (Fig. 2b) means that some sulphato groups are also present in the crystalline sample. Under the assumption that crystalline xerogel is a mixture of nickel(II) acetate tetrahydrate and nickel(II) sulfate heptahydrate, the mass ratio of the two components can be determined as 93.7 : 6.3. The XRD spectrum of crystalline xerogel does not reveal any peaks of nickel(II) sulfate heptahydrate. The reason is probably the poor crystallinity. The calculated weight loss up to 900 °C for a mixture of 93.7% nickel(II) acetate tetrahydrate and 6.3% of nickel(II) sulphate hexahydrate is 70.1% and is in excellent accordance with the observed one. The calculated weight loss during dehydration process of the described mixture is 29.9% and the measured one 34.1%. The observed difference can be ascribed to the fact that thermal decomposition of acetate groups starts before the dehydration process is complete [38]. To prove both statements, a sample of the same ratio of both components was prepared and a dynamic TG measurement was made. The obtained

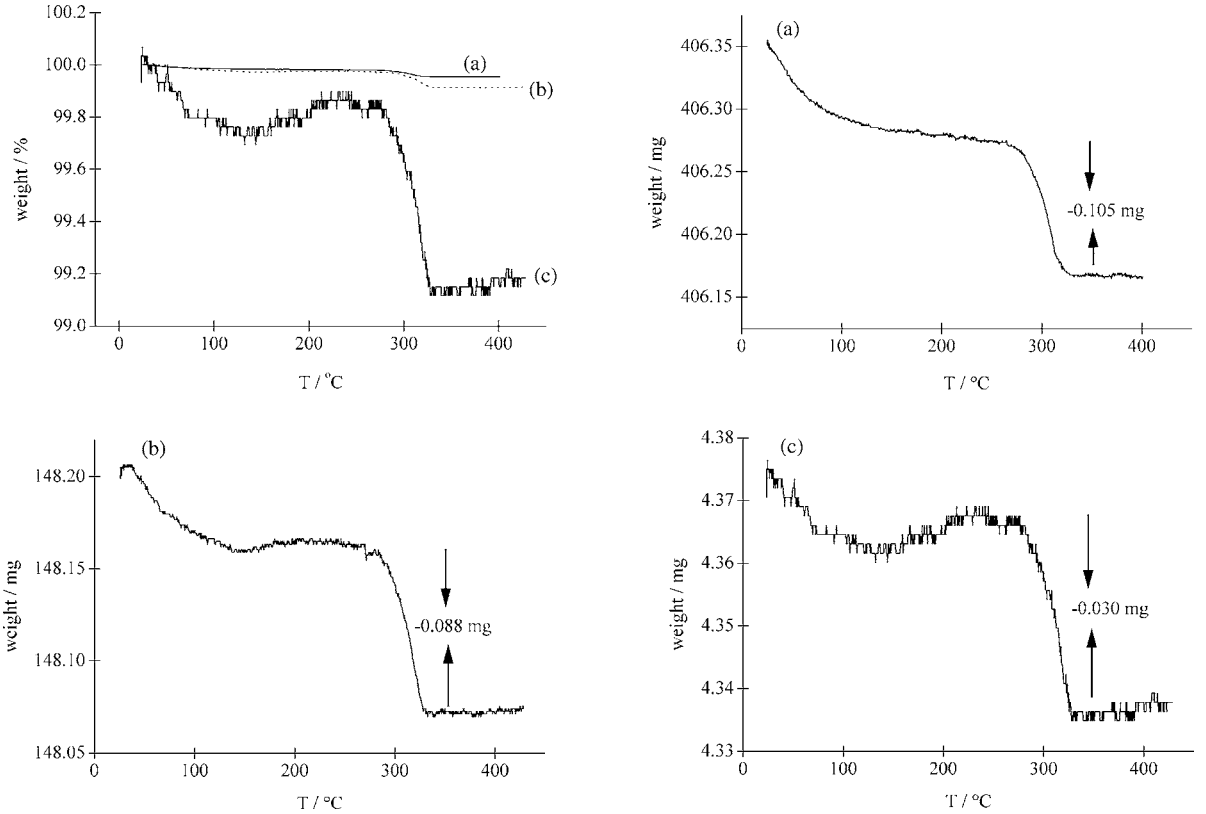

Fig. 5. Dynamic thermogravimetric curves of a thin film (percentage scale), deposited on an object glass (a), a microscope cover glasses (b) and an aluminium foil (c).

TG curve is nearly identical to that of the crystalline xerogel.

XRD analysis of films with a typical thickness of 100 nm gave only the substrate glass signal. To find out whether the structure of the thin film is crystalline or amorphous, EXAFS analysis of the amorphous xerogel and of the thin film deposited on an aluminium substrate was carried out. Apart from a higher degree of noise in the thin film signal, the spectra are identical, indicating the amorphous structure of the thin films [39].

Dynamic thermogravimetric curves of the thin film deposited on different substrates are shown in Fig. 5. Thermal decomposition of acetato groups leads to a clear step around 300 °C in thin film samples. On the assumption that the amorphous powder loses 34.5% of its weight in this temperature range, we can calculate the initial mass of the thin film from this weight change. The substrate to film mass ratio (*S*/*F*) and the initial mass of the film deposited per square centimeter substrate (*m*/*A*) can also be simply determined (Table 1). The signal on a percentage scale is greater in the case of lighter substrates. When aluminium foil was used, the weight loss was around 1% (Fig. 5c). The value of 0.1% weight loss was observed for

Table 1
Initial mass of sample, calculated substrate/thin film (*S*/*F*) mass ratio and the initial mass of thin film deposited per square centimeter of substrate (*m*/*A*) for different types of substrates

Type of substrate	Initial mass of the sample (thin film + substrate) (mg)	*S*/*F*	*m*/*A* (mg cm^{-2})
Microscope slide glass	406.352	1350	0.1
Microscope cover glass	148.199	580	0.064
Aluminium foil	4.373	50	0.06

microscope cover glass substrates (Fig. 5b) and only 0.04% for slide glass substrates (Fig. 5a). In contrast, the largest weight loss (0.105 mg) occurred during thermal decomposition of a thin film deposited on an slide glass. The reason is that because of the massive substrate the thin film was deposited in two layers successively; and this is obvious also from the *m*/*A* value (Table 1). When the observed weight loss is very small (0.030 mg, Fig. 5c), the buoyancy effect due to small variations in gas flow still remains.

Isothermal TG curves of the thin film and the corresponding xerogel at 270 and 300 °C are presented in Fig. 6. Both temperatures were chosen on the basis of dynamic measurements (Fig. 2). After isothermal treatment the temperature in the furnace was increased to 350 °C where decomposition is complete for both types of samples (thin film and xerogel). From the ratio of the isothermal weight loss after a defined time and the weight loss associated with decomposition of all acetato groups, the degree of thermal decomposition of acetates can be estimated. When thin films were exposed to 270 °C, the degree of thermal decomposition was 50% after 15 min, 80% after 30 min and 100% after 60 min (Fig. 6a). As we mentioned earlier, the formation of nickel oxide takes place at the same time. At 270 °C, only 30% decomposition of amorphous

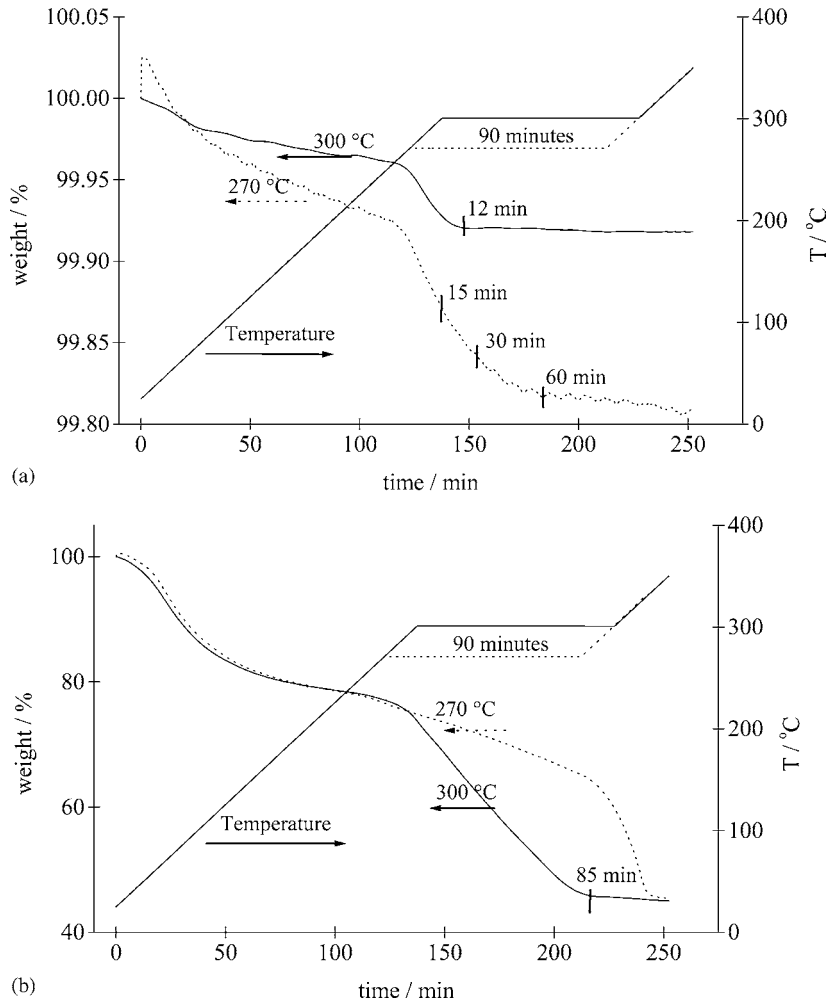

Fig. 6. Isothermal TG curves of the thin film (a) and corresponding xerogel (b) at 270 and 300 °C.

xerogel was observed after 60 min (Fig. 6b). From the same graph we can see that thermal decomposition of xerogel at 300 °C was finished after 85 min, whereas for the thin film it was complete after 12 min. Thin films with different ratios between the thermally undecomposed amorphous phase and nickel oxide can be prepared by controlling the time of heat treatment at 270 °C. At 300 °C, the decomposition process is much faster.

Both SDTA (single DTA, SDTA; with a thermocouple placed under the thermobalance sample holder) and DSC curves start around 300 °C (Fig. 7) and reflect the fact that volatiles produced react further with the gas stream in an exothermic manner [40]. The gas atmosphere generated during thermal decomposition influences the reaction itself. In TG/SDTA measurement the sample crucible was not covered and the gases released during decomposition could easily escape. An exothermic peak occurred at 311 °C. In DSC measurement, where the sample was covered with a pierced lid, the exothermic peak shifted toward higher temperature (370 °C). When DSC measurements of the thin film were made in open and partially closed (classical DSC measurement) systems, different onset temperature temperatures were also recorded, as well above mentioned effect (Fig. 8). A possible reason is that the better thermal conductivity of

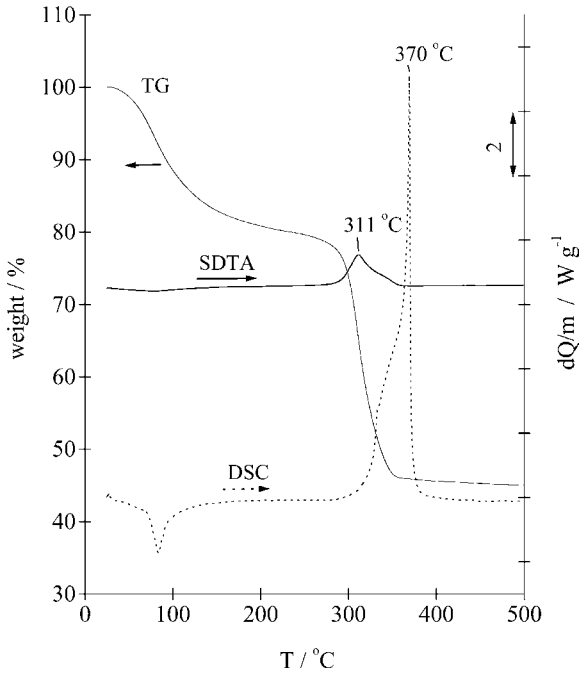

Fig. 7. Dynamic TG/SDTA and DSC curves of the amorphous xerogel under an air atmosphere.

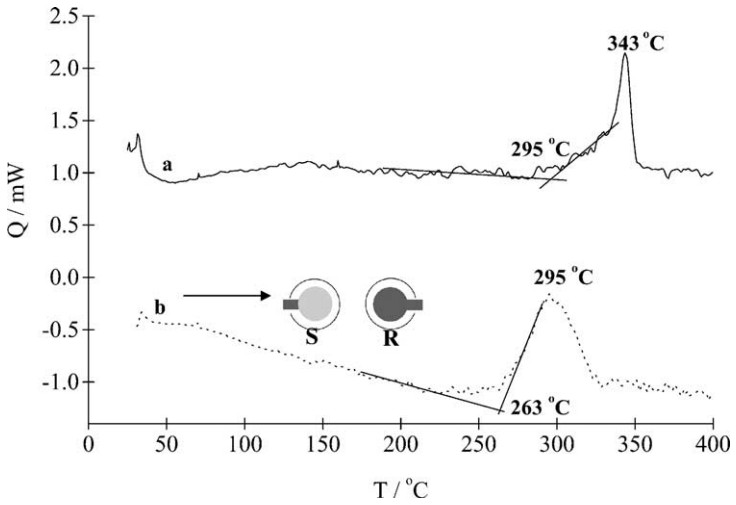

Fig. 8. DSC curves of a thin film deposited on aluminium foil, cut into small pieces, placed in an Al pan and covered with a pierced lid (a), and a thin film deposited on a platinum disc (diameter 6 mm) and placed directly on the DSC thermocouple (b). In the latter case, an identical platinum disc without a deposited film served as a reference.

platinum (0.716 $W\,cm^{-1}\,K^{-1}$) as compared to aluminium (0.243 $W\,cm^{-1}\,K^{-1}$) results in the exothermic signal starting at a lower temperature. For the thin film sample and the xerogel, the shape of the exotherm is characteristic of partially closed and open systems. The process seems to be somewhat retarded when the sample is covered. When the sample is uncovered, the shape of the exothermic change is quite symmetric.

In our case, thin films prepared for spectroelectrochemical measurements were always placed in a muffle furnace and then thermally treated in an open system. On the basis of the results obtained during this study, we can conclude that it is important to study the thermal process under the same circumstances as when processing on a large scale is performed.

The monochromatic spectral transmittance changes ($\lambda = 480$ nm) detected during CV measurements for thin films thermally treated to a different extent are shown in Fig. 9 (1st cycle) and Fig. 10 (100th cycle). During the anodic scan the oxidation of Ni^{2+} to Ni^{3+} causes colouration of the film and consequently the transmittance decreases. In the reverse scan, the reduction of Ni^{3+} leads to bleaching of the film. The maximal change in transmittance between the coloured and the bleached state in the 1st cycle was exhibited by a film heat treated for 15 min at 270 °C (43.1%, Table 2). However the decrease in the transmittance of the film in its bleached state by 1.9% at the end of the cycle shows that the reduction is not totally reversible. Films heat treated for 30 or 60 min at the same

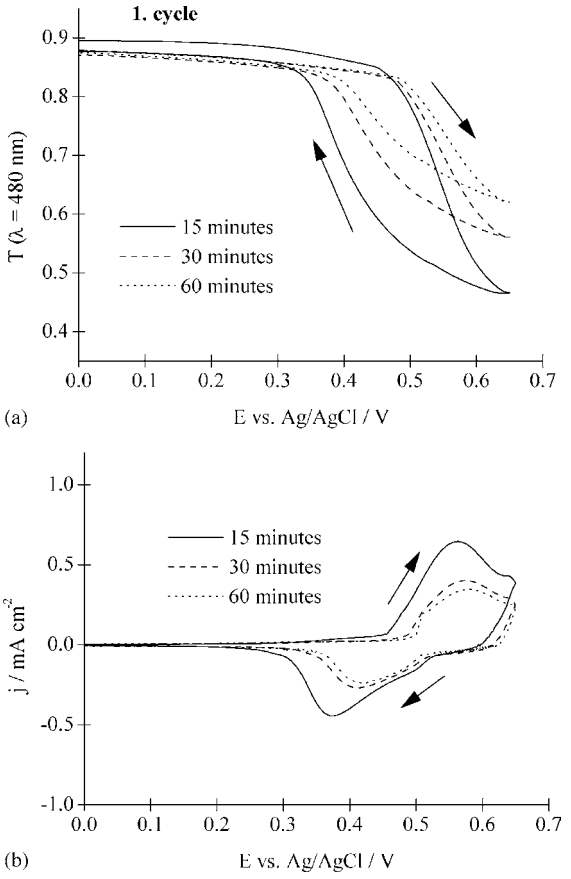

Fig. 9. Monochromatic transmittance changes (a) and cyclovoltammetric curves (b) of 35 nm thick nickel oxide films thermally treated to a different extent in 0.1 M LiOH—1st cycle.

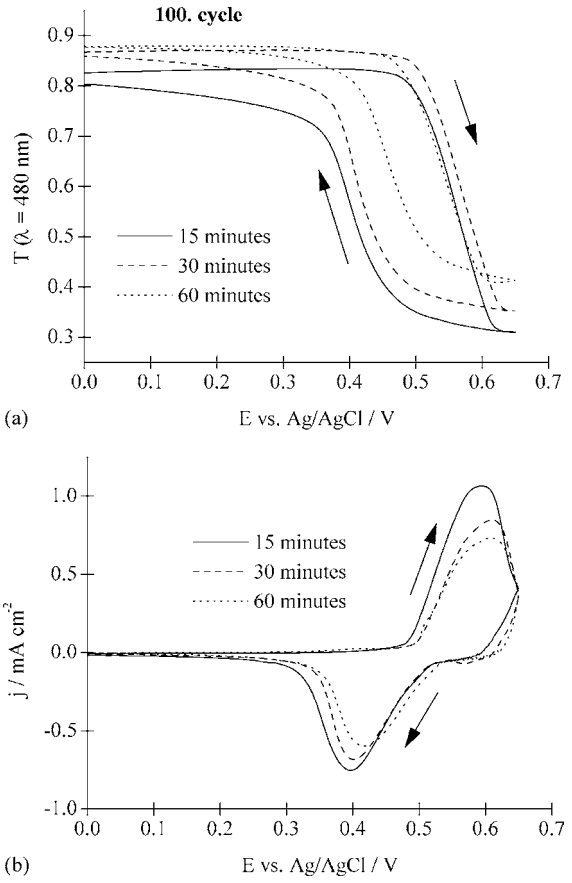

Fig. 10. Monochromatic transmittance changes (a) and cyclovoltammetric curves (b) of 35 nm thick nickel oxide films thermally treated to a different extent in 0.1 M LiOH—100th cycle.

Table 2
Position of the anodic and the cathodic peaks (E_p), maximal current densities (j_p), the ratio between the cathodic and the anodic charge (Q_C/Q_A) and the transmittance value ($\lambda = 480$ nm) at the beginning and at the end of the cycle

	1st cycle		100th cycle	
	Oxidation	Reduction	Oxidation	Reduction
15 min at 270 °C				
E_p (V)	0.56	0.37	0.59	0.40
j_p (mA cm^{-2})	0.64	−0.44	1.07	−0.75
Q_C/Q_A	0.66		0.79	
T ($\lambda = 480$ nm)	0.896 → 0.466	0.466 → 0.877	0.825 → 0.310	0.310 → 0.803
30 min at 270 °C				
E_p (V)	0.57	0.41	0.61	0.40
j_p (mA cm^{-2})	0.40	−0.26	0.85	−0.68
Q_C/Q_A	0.70		0.89	
T ($\lambda = 480$ nm)	0.897 → 0.561	0.561 → 0.871	0.867 → 0.352	0.352 → 0.858
60 min at 270 °C				
E_p (V)	0.58	0.42	0.61	0.42
j_p (mA cm^{-2})	0.35	−0.23	0.73	−0.59
Q_C/Q_A	0.68		0.90	
T ($\lambda = 480$ nm)	0.879 → 0.6217	0.621 → 0.874	0.878 → 0.413	0.413 → 0.877

temperature possess better reversibility (Fig. 9a). CV measurements of these films (Fig. 9b) are in accordance with the observed optical properties. The higher current densities indicate a greater number of active nickel ions for the least heat treated film, and the positions of the anodic and cathodic peaks (Table 2) reveal a more compact structure in those films exposed for 30 or 60 min to 270 °C. During the cycling process the number of active nickel ions increases: in the 100th cycle current densities are approximately 2.5 times higher than in the 1st cycle (Fig. 10b). A film which was exposed 60 min to 270 °C exhibited excellent reversibility in 100th cycle. The ratio between the cathodic and anodic charge (Q_C/Q_A) was 0.90 (Table 2). The transmittance change of 46.5% was smaller than for a thin film kept for 30 min at the same temperature (51.5%), but the latter did not bleach to the initial value in the 100th cycle (Fig. 10a).

4. Conclusions

For the thin film, thermal decomposition of organics starts at a lower temperature than for the corresponding xerogel. By regulating the time of heat treatment at 270 °C a set of thin films with different ratios between the thermally undecomposed amorphous phase and nanocrystalline nickel oxide can be prepared. A higher degree of heat treatment ensures better reversibility during the cycling process. A film exposed to an isothermal temperature for 15 min (decomposition of acetato groups 50%), does not bleach to the initial state even in the 1st cycle. The reversibility of a film thermally treated for 30 min at 270 °C, (decomposition of acetato groups 80%) is good in the 1st cycle, but diminishes up to the 100th cycle. A film, in which thermal decomposition of acetato groups is complete (60 min at 270 °C) possesses excellent reversibility. The structure of the film consists of nanocrystalline nickel oxide with sulphate ions monodentately bonded to nickel cations. The thermal decomposition of the amorphous xerogel is finished after 85 min at 300 °C. At this temperature the thin film decomposes in 12 min and the process is too fast to control the stoichiometry.

Acknowledgements

This work was supported by Grant PO-0508-0103 from the Ministry of Education, Science and Sport of the Republic of Slovenia. The authors wish to thank Barbara Novosel, M.Sc., for EGA measurements.

References

[1] K. Bange, T. Gambke, Adv. Mater. 2 (1990) 10.
[2] A.R. West, Solid State Chemistry and its Application, Wiley, Chichester, 1985, p. 515.
[3] J. He, H. Lindström, A. Hagfeldt, S.-E. Lindquist, J. Phys. Chem. B 103 (1999) 8940.
[4] A. Nemetz, A. Temmink, K. Bange, S. Cordoba de Torresi, C. Gabrielli, R. Torresi, A. Hugot-Le Goff, Sol. Energy Mater. Sol. Cells 25 (1992) 93.
[5] M. Gómez, A. Medina, W. Estrada, Sol. Energy Mater. Sol. Cells 64 (2000) 297.
[6] M.C. Fantini, G.H. Bezerra, C.R. Carvalho, A. Gorenstein, SPIE Proc. 1536 (1991) 81.
[7] M.C. Fantini, A. Gorenstein, Sol. Energy Mater. Sol. Cells 16 (1987) 487.
[8] J. Scarminio, A. Urbano, B.J. Gardes, A. Gorenstein, J. Mater. Sci. Lett. 11 (1992) 562.
[9] W. Estrada, A.M. Andersson, C.G. Granqvist, J. Appl. Phys. 64 (1988) 3678.
[10] A. Gorenstein, F. Decker, M. Fantini, W. Estrada, SPIE Proc. 4 (1988) 272.
[11] A.M. Andersson, W. Estrada, C.G. Granqvist, A. Gorenstein, F. Decker, SPIE Proc. 1272 (1990) 96.
[12] K. Yoshimura, T. Miki, S. Tanemura, Jpn. J. Appl. Phys. 34 (1995) 2440.
[13] Z. Xuping, C. Guoping, Thin Solid Films 298 (1997) 53.
[14] T. Miki, K. Yoshimura, Y. Tai, M. Tazawa, P. Jin, S. Tanemura, in: Proceedings of the Third IUMRS International Conference on Advanced Materials, Tokyo, Japan, 31 August–4 September 1993 (article no. KP12).
[15] A. Šurca, B. Orel, B. Pihlar, P. Bukovec, J. Electroanal. Chem. 408 (1996) 83.
[16] X. Chen, X. Hu, J. Feng, Nanostruct. Mater. 6 (1995) 309.
[17] M. Chigane, M. Ishikawa, J. Electrochem. Soc. 141 (1994) 3439.
[18] R.M. Torresi, M.V. Vázquez, A. Gorenstein, S.I. Córdoba de Torresi, Thin Solid Films 229 (1993) 180.
[19] C. Natarajan, H. Matsumoto, G. Nogami, J. Electrochem. Soc. 114 (1997) 121.
[20] P.K. Sharma, M.C.A. Fantini, A. Gorenstein, Solid State Ionics 113–115 (1998) 457.
[21] L. Županc-Mežnar, B. Praček, B. Orel, P. Bukovec, Thin Solid Films 317 (1998) 336.
[22] L. Niinistö, J. Therm. Anal. Cal. 56 (1999) 7.
[23] W.W. Wendlandt, Thermal Methods of Analysis, Interscience, New York, 1964, p. 17.
[24] R. Cerc Korošec, P. Bukovec, J. Therm. Anal. Cal. 56 (1999) 587.
[25] A. Šurca, B. Orel, R. Cerc-Korošec, P. Bukovec, B. Pihlar, J. Electroanal. Chem. 433 (1997) 57.
[26] A. Šurca, B. Orel, B. Pihlar, J. Solid State Electrochem. 2 (1998) 389.
[27] G. Boschloo, A. Hagfeldt, J. Phys. Chem. B 105 (2001) 3039.
[28] M. Leskelä, T. Leskelä, L. Niinistö, J. Therm. Anal. Cal. 40 (1993) 1077.
[29] P.K. Gallagher, J. Therm. Anal. 38 (1992) 17.
[30] S. Lieb, R.K. MacCrone, J. Theimer, E.W. Maby, J. Mater. Res. 1 (1986) 792.
[31] J. Przyluski, J. Plocharski, W. Bujwan:, J. Therm. Anal. 21 (1981) 235.
[32] S. Hackwood, G. Beni, P.K. Gallagher, Solid State Ionics 2 (1981) 297.
[33] P.S. Gill, S.R. Sauerbrunn, B.S. Crowe, J. Therm. Anal. 38 (1992) 255.
[34] F. Nava, G. Ottaviani, G. Riontino, Mater. Lett. 3 (1985) 3113.
[35] K. Nakamoto, Infrared and Raman Spectra of Inorganic and Coordination Compounds, 5th ed., Part B, Wiley, New York, 1997, pp. 59, 60.
[36] K. Nakamoto, Infrared and Raman Spectra of Inorganic and Coordination Compounds, 5th ed., Part B, Wiley, New York 1997, pp. 80, 81.
[37] C. Faure, C. Delmas, M. Fouassier, J. Power Sources 35 (1991) 279.
[38] M.A. Elmasry, A. Gaber, E.M. Khater, J. Therm. Anal. 47 (1996) 757.
[39] R. Cerc Korošec, Dissertation, Ljubljana, 2001, p. 108.
[40] P.K. Gallagher, Thermogravimetry and thermomagnetometry, in: M.E. Brown (Ed.), Handbook of Thermal Analysis and Calorimetry, vol. 1, Elsevier, Amsterdam, 1998, p. 262.